One Nanometer Resolution Electrical Probe via Atomic Metal Filament Formation

Seung Sae Hong,[†] Judy J. Cha,[‡] and Yi Cui*,[‡]

[†]Department of Applied Physics and [‡]Department of Materials Science and Engineering, Stanford University, Stanford, California 94305

ABSTRACT Scanning probe microscopy has been widely used to investigate various interactions in microscopic nature. Particularly, conductive atomic force microscopy (C-AFM) can provide local electronic signals conveniently, but the probe resolution of C-AFM has been limited by the tip geometry. Here, we improve the probe resolution greatly by forming an atomic-size metallic filament on a commercial C-AFM tip. We demonstrate ~1 nm lateral resolution in C-AFM using the metal filament tip. The filament tip is mechanically robust and electrically stable in repeated scans under ambient conditions since it is imbedded in a stable insulating matrix. The formation of the atomic filament is highly controllable and reproducible and can be easily integrated to existing AFM tip technologies to produce the next generation of high-resolution electrical and other scanning probes.

KEYWORDS Atomic metal filament, scanning probe microscopy, advanced probe, resistive switching.

Among various interaction forces and signals scanning probe microscopy (SPM) can detect from a sample surface,[1−16] electrical current is one of the primary signals used to study materials properties. Two SPM techniques, scanning tunneling microcopy (STM) and conductive atomic force microscopy (C-AFM), are widely used to detect electrical signals from a sample surface. STM is based on the tunneling current measurement and can provide electronic information at atomic resolution, but it requires a conducting substrate and/or ultrahigh vacuum. C-AFM, on the other hand, measures electrical current in direct contact with the surface, providing explicit local conductivity information in an ambient condition without a conducting substrate.

Although C-AFM shows angstrom-scale sensitivity in a vertical direction, its lateral resolution is generally 100 times larger than atomic scale.[3] Typically, the lateral resolution of AFM is limited by the size of a microfabricated tip except when detecting short-range (<1 nm) chemical force interactions.[4−6] As such, electrical signals that modulate at length scales below ~10 nm in lateral dimensions cannot be resolved with conventional C-AFM. To improve the lateral resolution, microfabricated tips can be modified. For example, carbon nanotube (CNT) tips achieve markedly improved resolution in topographic imaging.[7−9] However, difficulties in fabrication, large contact resistance, and fragility during usage limit wider applications of CNT tips.[9,10] In order to overcome the limitations of CNT tips, it is essential for a new nanostructure probe to be easily integrated with the existing probe technology and be mechanically and electrically robust, while enabling ultrahigh lateral resolution.

In this Letter, we demonstrate a new type of C-AFM tip based on atomic metal filament formation and show that the lateral resolution can be greatly improved. The formation of a filamentary conduction path in a metal−insulator−metal (MIM) structure has been known since the 1960s and shows great potential as diverse electronic devices.[16−23] One of the switching mechanisms is metallic filament formation, where cations from one metal electrode form a single conducting path of atomic dimensions in a thin insulator gap.[21] By exploiting these features of the metallic filament formation, we design a high-resolution C-AFM probe tip made of a nonvolatile and atomic size metal filament. The atomic metal filament is imbedded in an insulating layer on a conventional AFM tip and one end of the filament is exposed to convey surface signals (i.e., electric current or forces). The localized current path (the atomic filament) can detect current signals at much higher lateral resolution than conventional C-AFM tips. Moreover, the formation of the metal filament is highly controllable by controlling the electrical bias applied to the tip precisely, which results in the easiness and excellent reproducibility of the tip fabrication.

To build an atomic filament on an AFM tip, we designed a detachable MIM structure. We form only the metal−insulator (MI) junction on the AFM tip by depositing an amorphous aluminum oxide layer (insulator) uniformly on a C-AFM tip (metal) by atomic layer deposition (ALD). Once the coated tip touches a metallic surface, a complete MIM configuration is formed at the end of the AFM tip (Figure 1a,b). With a bias (~3 V), metal ions created by electrochemical oxidation of the bottom electrode (positive voltage) penetrate into the alumina layer (Figure 1c). The atomic filament reaches the upper electrode (C-AFM tip) driven by the electrostatic force, and metal atoms accumulate at the end of the C-AFM tip by electrochemical reduction (Figure 1d). Finally, the metal filament has a taper shape with only a few metal atoms
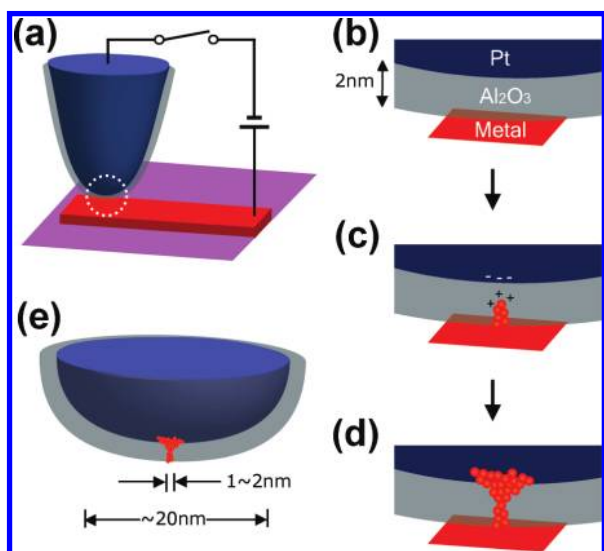
FIGURE 1. Schematic of the metallic filament formation on the AFM probe. (a) A conventional C-AFM tip with alumina coating contacts the bottom metal and makes a local MIM junction. The MIM junction surface (dotted line) is naturally located at the geometric minimum of the whole tip. (b) Detachable MIM structure with the Pt-coated AFM tip (M), amorphous alumina (I), and the metal surface (M). Here we focus on palladium (Pd) metal layer surface, but we also observed that various metals exhibit the same switching characteristics. (c) With positive bias on the metal layer, metal ions penetrate into the amorphous layer driven by electric field. (d) Metal ions keep accumulating on Pt surface of the AFM tip while maintaining good electrical contact. (e) The diameter of the atomic filament ($1-2$ nm) is significantly smaller than the original tip size (~ 20 nm).

exposed at the apex (Figure 1e), which collects electrical signals from the sample surface with much smaller interacting volume resulting in improved lateral resolution.

Filament tips of different metals—from magnetic to noble metals—can be easily made with nearly 100% yield (over 50 filament C-AFM tips were fabricated). (See Supporting Information.) Here we focus on palladium (Pd) as an example to demonstrate the metal filament tip. The Pd filament has been observed to be stable for more than a month as embedded in the insulating matrix. In the C-AFM mode, the filament tip can easily be used to image various nanoscale structures, such as nanocrystals, nanowires, and CNTs.

To confirm the metal filament formation at the end of the AFM tip, we imaged the tip using a transmission electron microscopy (TEM) and energy dispersive X-ray spectroscopy (EDX). Scanning EDX provides elemental maps of the tip with nanoscale spatial resolution. The platinum (Pt) map (Figure 2f) has exactly the same shape as the tip image (Figure 2e) as expected because the C-AFM tip was Pt-coated. Also, a thin aluminum oxide layer, uniformly coating the AFM tip, is clearly visible in Figure 2e. In contrast to the Pt map, the Pd map shows that Pd atoms are confined to a small region at the tip end (Figure 2g). A series of EDX mappings confirm that the Pd metal ions are stable under the focused electron beam and they are confined within ~ 4 nm. We believe that this Pd map is mainly from the accumulated Pd atoms at the larger base of the taper filament
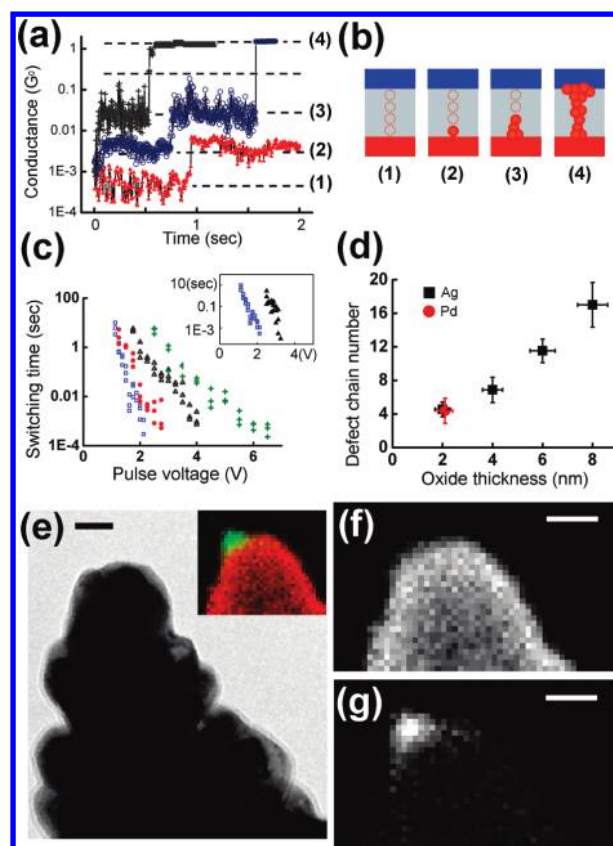

FIGURE 2. Electrical measurement of the metallic filament formation. (a) Junction tunneling conductance changes in a stepwise fashion during Pd filament formation in the alumina film (2 nm) with bias of 2.5 V. Initial time interval before switching is not shown in this plot. Different time scales are used for three data sets to avoid plot overlap. The rescale factors of data sets are $2\times$ slower (black plus signs), $4\times$ slower (blue circles), and $1\times$ (red solid triangles). All values are scaled to a unit of the quantum conductance $G_0 = 2e^2/h$. The change in quantized tunneling conductance implies that metal ions sequentially hop along the chain of defect sites. (b) A schematic of sequential growth of the Pd filament in 2 nm oxide layer to describe the quantized tunneling conductance in (a). Each state from (1) to (4) would be matched well with the plateau of the tunneling conductance (1)−(4) in (a). (c) Switching time as a function of different pulse voltages (Ag filament formation) at different thicknesses of alumina. The switching time is defined as the time interval between the initial voltage applied and the first conductance jump. The exponential relation between the time and the pulse voltage implies that the filament formation is due to the thermal activation of metal ions. Four different thicknesses of alumina, 2 nm (blue open box), 4 nm (red solid circle), 6 nm (gray open triangle), and 8 nm (green plus sign), are shown. The inset in (c) shows a time−voltage relation of different metals, Ag (blue open box) and Pd (black solid triangle) filament formation in 2 nm alumina layer, whose slopes are the same but the voltage is very different. (d) The defect site chain numbers calculated from the slope in (c) is proportional to the thickness of the alumina layer. Detailed analysis is described in the Supporting Information. (e) TEM image of the filament tip. Alumina layer covers the entire tip surface except the very end part, where the layer disappeared after the electron beam scan for scanning EDX (see Supporting Information for more analysis). The elemental map (inset of (e), combined image from (f) and (g), artificially colored) shows dramatic contrast of Pt (red) and Pd (green), which confirms the composition of the metallic nanostructure. (f, g) EDX signal map of Pt (f) and Pd (g). The Pt map (f) has exactly the same shape as the tip image (e) because the original tip is made of Pt coating on a silicon tip. All the scale bars indicate 10 nm.
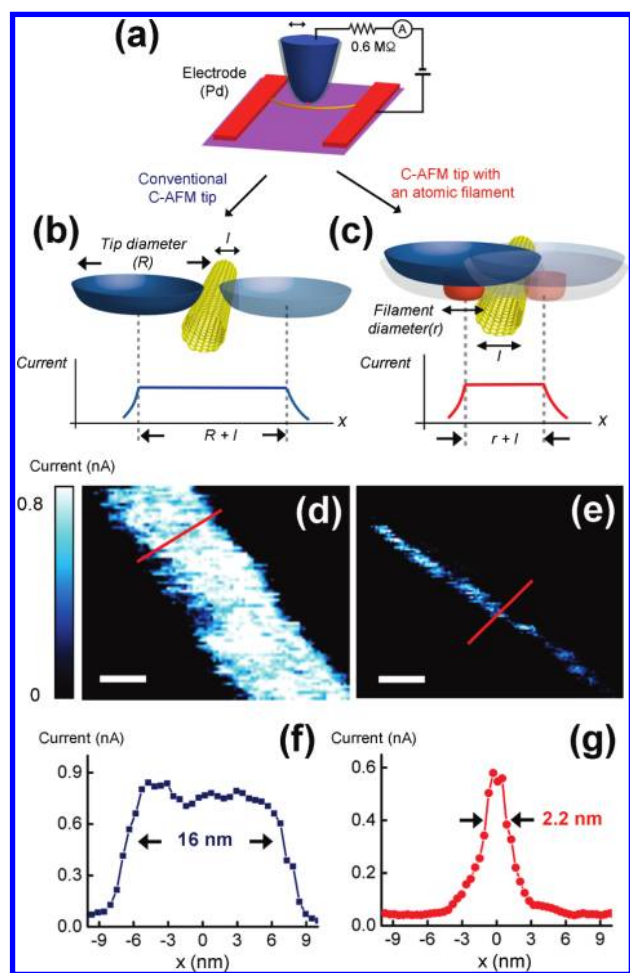
FIGURE 3. Conductive scan experiment of a nanoscale object (swCNT) by two different tips. (a) Experimental setup for conductive scans in contact mode. Pd electrodes were patterned on the swCNT for electrical contact. The applied bias during the scan (0.5 ± 0.1 mV) is much smaller than the normal switching voltage (~ 3 V) so that the existing Pd filament is stable during conductive scans. (b, c) Schematic to show the convolution of conductive images. (b) If the tip size (R) is much larger than the feature size (l), then the lateral size of the conductive image ($R + l$) is determined by the tip size (R). (c) In the case of the Pd filament tip, the convolution can be minimized due to the small dimension of the filament (r) and the image size ($r + l$) will be close to the original feature size (l). In both cases, the tip/filament size (R or r) would be the resolution of each probe. (d−g) Conductive scan images and their line cuts of a swCNT, scan by the normal C-AFM tip (d, f) and by the Pd filament tip (e, g). Scale bars indicate 10 nm. From the line cut (f), the estimated size of the tip (R) is about 15 nm (16 nm − 1.3 nm), where 1.3 nm is the diameter of the swCNT (l). From another line cut (g), we also estimate the filament size (r) as 0.9 nm (2.2 nm − 1.3 nm).

(Figure 1d) rather than the smaller end of the atomic filament itself, which is about 1 nm based on the conductive scans (Figure 3).

The atomic filament formation can be explained as the thermally activated ion penetration, with applied bias lowering the activation barrier.[22,23] Because the amorphous matrix has defects at the atomic scale, metal ions can keep "jumping" into a chain of energetically favorable defect sites in the amorphous matrix (schematic in Figure 2b). Hence,

the conductance during the filament formation will have discrete changes as the defect sites get filled. Figure 2a shows the tunneling conductance between the growing filament and the opposite electrode. Interestingly, it always ascends stepwise with a uniform step size in logarithmic scale. Since tunneling conductance depends exponentially on the tunneling distance,[24] the discrete tunneling conductance corresponds to the stepwise growth of the filament along the defect sites in the chain (Figure 2b). At varying thicknesses of the amorphous matrix, we measured the switching time as a function of the applied bias. As expected, it takes longer to form a conductive path in a thicker amorphous matrix (Figure 2c) as there would be more defect sites to fill in the thicker amorphous matrix. Additionally, we observe that the switching time (τ) depends exponentially on the applied bias (V) (Figure 2c,d) illustrating the activation process of metal ions to form the atomic filament. (See Supporting Information.) This stepwise growth implies that the atomic filament can be built in a controllable manner. Such atomic length control of filament formation will be a very powerful technique for general nanoengineering, as well as for the fabrication of the advanced scanning probes.

With the metallic filament formed on a C-AFM tip, we imaged a nanometer size feature—single wall carbon nanotubes (swCNTs)—to estimate the lateral resolution of the Pd filament tip. In addition, the same nanotube was imaged with a normal C-AFM tip for comparison. By applying a small bias to the two different tips, topographic and conductive signals were simultaneously acquired in contact mode (Figure 3a). Both topographic and conductive maps are a convolution of the tip and the sample, which means the lateral resolution of the scan is determined by the tip size. In topographic maps, the apex diameters of the normal C-AFM tip and the filament tip are similar; thus we expect the apparent diameter of the imaged swCNT in topographic maps to be the same. However, in the conductive maps, the diameter of the swCNT acquired with the filament tip will be much smaller as the interacting volume to obtain electrical signals is confined to the metal filament (Figure 3b,c).

Panels d and e of Figure 3 show the conductive maps of the swCNT acquired by two different tips, showing drastic difference in the diameter of the mapped swCNT. The diameter of the swCNT scanned by the normal C-AFM tip (Figure 3d) is 16 nm wide. From height measurement, we estimate the actual diameter of the swCNT to be ~ 1.3 nm. (See Supporting Information.) Hence, the apparent swCNT diameter of 16 nm using the C-AFM tip is due to the large C-AFM tip diameter (~ 15 nm). In the filament tip's case (Figure 3e), the swCNT diameter is only 2.2 nm wide, which is very close to the original size of the swCNT. Parts f and g of Figure 3 are line profiles obtained from panels d and e of Figure 3, respectively. Considering the convolution effect with the tip, we estimate that the filament is about 0.9 nm wide, which determines the resolution of the conductive
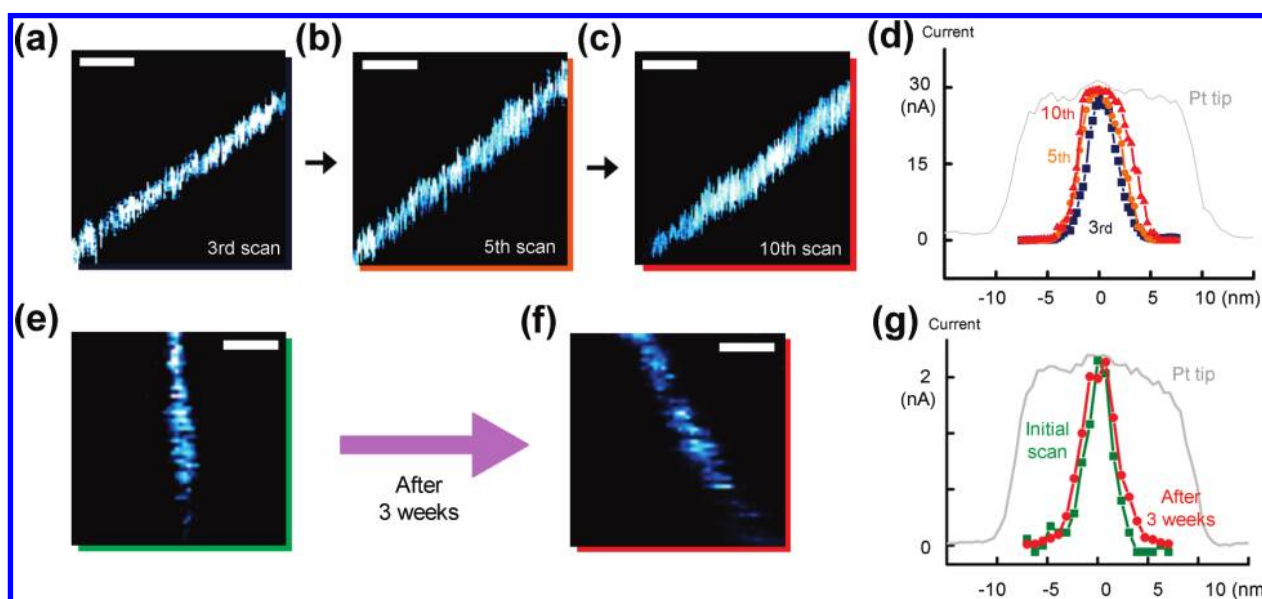
FIGURE 4. (a−c) Conductive images of identical swCNT from repeated scans by single Pd filament tip: third scan, fifth scan, and tenth scan, respectively. (d) The line cuts of multiple scan images (a−c). Gray line is from the swCNT image scanned by a normal C-AFM tip, which is not shown in this figure. (e, f) Conductive images of identical swCNT from initial scan (e) and the scan after 3 weeks (f) using the same Pd filament tip. (g) Line cuts indicate that the filament was stable for a long period of time and the resolution was barely changed.

scan. Compared with the original C-AFM resolution (∼15 nm), the resolution is improved more than 10 times by the atomic filament tip. This nanometer resolution is possible because only the small end of the atomic filament detects the electrical signal, regardless of the size of the AFM tip covered by insulating alumina layer. Details of conductive scans such as contact resistances and current can be found in the Supporting Information.

Repeatable scanning and stability test of the filament tip show that the metallic filament is stable during multiple scans and for a long period. We scanned a swCNT with the same tip multiple times and observed only a small change in the measured diameter of the nanotube between the scans (Figure 4a−d). During the first 10 repeated scans on the same nanotube, the diameter of the swCNT slightly increased, which may be due to partial abrasion of the insulating alumina layer. But even after 10 scans, the tip maintains high resolution (estimated to be ∼5 nm, extracted from deconvolution of the apparent swCNT diameter with the true diameter of the swCNT), which is still much better than the normal tip without a metallic filament (Figure 4d). We also tested the filament tip stability. After scanning a swCNT once, we repeated the same scan using the same tip on the identical nanotube 3 weeks later (Figure 4e−g). The image of the swCNT did not change much, indicating that the metal filament is stable for a long time, thus maintaining the high resolution. This suggests that the filament tip can be used as a real application in scanning force microscopy.

In summary, we have demonstrated a novel electrical probe constructed by a stepwise atomic filament growth. With minimal fabrication steps, atomic filaments of different metals including magnetic metals can be formed on a conventional C-AFM tip. The robust atomic structure achieves an ultimate 1 nm resolution conductive probe working at ambient conditions. This metallic filament is expected to improve various electrical and magnetic force SPMs[3,11−13] enough to investigate mesoscopic systems with higher resolution. The geometry of the filament is optimal for high-resolution electrochemical probes[25] and biological tip functionalization.[26,27] In addition, controllable atomic switching on the tip suggests a new possibility in scanning probe engineering, which will realize the ideal "lab on a tip".[3]

Supporting Information Available. Sample preparation method, characterization methods, and microwave/transport measurement details and additional force calculations and data. This material is available free of charge via the Internet at http://pubs.acs.org.

REFERENCES AND NOTES

(1) Binnig, G.; Rohrer, H.; Gerber, C.; Weibel, E. *Phys. Rev. Lett.* **1982**, *49*, 57.
(2) Binnig, G.; Quate, C. F.; Gerber, C. *Phys. Rev. Lett.* **1986**, *56*, 930.
(3) Meyer, E.; Hug, H. J.; Bennewitz, R. *Scanning probe microscopy: the lab on a tip*; Springer: Berlin and New York, 2004.
(4) Giessibl, F. J. *Science* **1995**, *267*, 68−71.
(5) Lantz, M. A.; Hug, H. J.; Hoffmann, R.; van Schendel, P. J. A.; Kappenberger, P.; Martin, S.; Baratoff, A.; Guntherodt, H. *Science* **2001**, *291*, 2580−2583.
(6) Sugimoto, Y.; Pou, P.; Abe, M.; Jelinek, P.; Perez, R.; Morita, S.; Custance, O. *Nature* **2007**, *446*, 64−67.

(7) Dai, H.; Hafner, J. H.; Rinzler, A. G.; Colbert, D. T.; Smalley, R. E. *Nature* **1996**, *384*, 147–150.

(8) Hafner, J. H.; Cheung, C. L.; Lieber, C. M. *Nature* **1999**, *398*, 761–762.

(9) Wilson, N. R.; Macpherson, J. V. *Nat. Nanotechnol.* **2009**, *4*, 483–491.

(10) Wilson, N. R.; Cobden, D. H.; Macpherson, J. V. *J. Phys. Chem. B* **2002**, *106*, 13102–13105.

(11) Topinka, M. A.; LeRoy, B. J.; Shaw, S. E. J.; Heller, E. J.; Westervelt, R. M.; Maranowski, K. D.; Gossard, A. C. *Science* **2000**, *289*, 2323–2326.

(12) Deng, Z.; Yenilmez, E.; Leu, J.; Hoffman, J. E.; Straver, E. W. J.; Dai, H.; Moler, K. A. *Appl. Phys. Lett.* **2004**, *85*, 6263.

(13) Rugar, D.; Budakian, R.; Mamin, H. J.; Chui, B. W. *Nature* **2004**, *430*, 329–332.

(14) De Angelis, F.; Das, G.; Candeloro, P.; Patrini, M.; Galli, M.; Bek, A.; Lazzarino, M.; Maksymov, I.; Liberale, C.; Andreani, L. C.; Di Fabrizio, E. *Nat. Nanotechnol.* **2010**, *5*, 67–72.

(15) Park, J.; Rosenblatt, S.; Yaish, Y.; Sazonova, V.; Üstünel, H.; Braig, S.; Arias, T. A.; Brouwer, P. W.; McEuen, P. L. *Nano Lett.* **2004**, *4*, 517–520.

(16) Lau, C. N.; Stewart, D. R.; Williams, R. S.; Bockrath, M. *Nano Lett.* **2004**, *4*, 569–572.

(17) Hickmott, T. W. *J. Appl. Phys.* **1962**, *33*, 2669.

(18) Dearnaley, G.; Stoneham, A. M.; Morgan, D. V. *Rep. Prog. Phys.* **1970**, *33*, 1129–1191.

(19) Waser, R.; Aono, M. *Nat. Mater.* **2007**, *6*, 833–840.

(20) Strukov, D. B.; Snider, G. S.; Stewart, D. R.; Williams, R. S. *Nature* **2008**, *453*, 80–83.

(21) Terabe, K.; Hasegawa, T.; Nakayama, T.; Aono, M. *Nature* **2005**, *433*, 47–50.

(22) Dong, Y.; Yu, G.; McAlpine, M. C.; Lu, W.; Lieber, C. M. *Nano Lett.* **2008**, *8*, 386–391.

(23) Jo, S. H.; Kim, K.; Lu, W. *Nano Lett.* **2009**, *9*, 496–500.

(24) Simmons, J. G. *J. Appl. Phys.* **1963**, *34*, 2581.

(25) Burt, D. P.; Wilson, N. R.; Weaver, J. M. R.; Dobson, P. S.; Macpherson, J. V. *Nano Lett.* **2005**, *5*, 639–643.

(26) Florin, E.; Moy, V.; Gaub, H. *Science* **1994**, *264*, 415–417.

(27) Chen, X.; Kis, A.; Zettl, A.; Bertozzi, C. R. *Proc. Natl. Acad. Sci.* **2007**, *104*, 8218–8222.